AFRL-RX-WP-TP-2012-0378

CALCULATION OF GROWTH STRESS IN SiO_2 SCALES FORMED BY OXIDATION OF SiC FIBERS (PREPRINT)

Randall S. Hay
Composites Branch
Structural Materials Division

JULY 2012
Interim

AIR FORCE RESEARCH LABORATORY
MATERIALS AND MANUFACTURING DIRECTORATE
WRIGHT-PATTERSON AIR FORCE BASE, OH 45433-7750
AIR FORCE MATERIEL COMMAND
UNITED STATES AIR FORCE

REPORT DOCUMENTATION PAGE

Form Approved
OMB No. 0704-0188

1. REPORT DATE *(DD-MM-YY)*	2. REPORT TYPE	3. DATES COVERED *(From - To)*
July 2012	Technical Paper	1 June 2012 – 1 July 2012

4. TITLE AND SUBTITLE

CALCULATION OF GROWTH STRESS IN SiO_2 SCALES FORMED BY OXIDATION OF SiC FIBERS (PREPRINT)

5a. CONTRACT NUMBER
In-house

5b. GRANT NUMBER

5c. PROGRAM ELEMENT NUMBER
62102F

6. AUTHOR(S)
Randall S. Hay (AFRL/RXCC)

5d. PROJECT NUMBER
4347

5e. TASK NUMBER
50

5f. WORK UNIT NUMBER
LN102102

7. PERFORMING ORGANIZATION NAME(S) AND ADDRESS(ES)

Composites Branch (AFRL/RXCC)
Structural Materials Division
Air Force Research Laboratory, Materials and Manufacturing Directorate
Wright-Patterson Air Force Base, OH 45433-7750
Air Force Materiel Command, United States Air Force

8. PERFORMING ORGANIZATION REPORT NUMBER
AFRL-RX-WP-TP-2012-0378

9. SPONSORING/MONITORING AGENCY NAME(S) AND ADDRESS(ES)

Air Force Research Laboratory
Materials and Manufacturing Directorate
Wright-Patterson Air Force Base, OH 45433-7750
Air Force Materiel Command
United States Air Force

10. SPONSORING/MONITORING AGENCY ACRONYM(S)
AFRL/RXCC

11. SPONSORING/MONITORING AGENCY REPORT NUMBER(S)
AFRL-RX-WP-TP-2012-0378

12. DISTRIBUTION/AVAILABILITY STATEMENT
Approved for public release; distribution unlimited. Preprint to be submitted to Ceramics Engineering and Science Proceedings.

13. SUPPLEMENTARY NOTES
The U.S. Government is joint author of this work and has the right to use, modify, reproduce, release, perform, display, or disclose the work. PA Case Number and clearance date: 88ABW-2012-0778, 14 February 2012. This document contains color.

14. ABSTRACT
A numerical method to calculate growth stress in SiO2 scales formed during SiC fiber oxidation is described. Calculations were done for SiC fibers between 700° and 1300°C using previously measured Deal-Grove parameters for oxidation kinetics and an Eyring viscoplastic model for SiO2 scale viscosity. Initial compressive stresses in SiO2 of ~25 GPa from the 2.2× oxidation volume expansion are rapidly relaxed to lower levels by flow of silica with a shear stress-dependent viscosity. At 700° - 900°C, axial and hoop stress at the GPa level persist. Radial expansion of the outer scale causes hoop stress to become tensile; axial stress becomes tensile by the Poisson effect. Tensile hoop stresses can be >2 GPa for thick scales formed at <1000°C. Effects of different fiber radii on growth stresses are examined. Limitations of the method and analytical approximations are discussed.

15. SUBJECT TERMS
SiC, Oxidation, Fibers

16. SECURITY CLASSIFICATION OF:			17. LIMITATION OF ABSTRACT:	NUMBER OF PAGES	19a. NAME OF RESPONSIBLE PERSON (Monitor)
a. REPORT	b. ABSTRACT	c. THIS PAGE			Randall Hay
Unclassified	Unclassified	Unclassified	SAR	12	19b. TELEPHONE NUMBER *(Include Area Code)* N/A

CALCULATION OF GROWTH STRESS IN SiO_2 SCALES FORMED BY OXIDATION OF SiC FIBERS

R. S. Hay
Air Force Research Laboratory
Materials and Manufacturing Directorate, WPAFB, OH

ABSTRACT

A numerical method to calculate growth stress in SiO_2 scales formed during SiC fiber oxidation is described. Calculations were done for SiC fibers between 700° and 1300°C using previously measured Deal-Grove parameters for oxidation kinetics and an Eyring viscoplastic model for SiO_2 scale viscosity. Initial compressive stresses in SiO_2 of ~25 GPa from the 2.2× oxidation volume expansion are rapidly relaxed to lower levels by flow of silica with a shear stress-dependent viscosity. At 700° - 900°C, axial and hoop stress at the GPa level persist. Radial expansion of the outer scale causes hoop stress to become tensile; axial stress becomes tensile by the Poisson effect. Tensile hoop stresses can be >2 GPa for thick scales formed at <1000°C. Effects of different fiber radii on growth stresses are examined. Limitations of the method and analytical approximations are discussed.

INTRODUCTION

Constraint of the 2.2× volume expansion during oxidation of SiC to SiO_2 generates very large growth stresses. Microstructural evidence for these stresses exists for crystalline scales on SiC fibers. High dislocation densities in crystalline SiO_2 near the SiC-SiO_2 interface suggest high shear stresses exist during growth of new crystalline scale.[1] Axial cracks form in the outer scale from tensile hoop growth stress.[1-3] Tensile growth stress in the scale may decrease fiber strength by surface nucleated fracture.[4] Residual stresses affect SiC fiber strength and are important for SiC-SiC ceramic matrix composites (CMCs) for high temperature structural applications.[5-6]

Growth stress during silicon oxidation, which has a volume expansion similar to that for SiC oxidation, has been extensively modeled.[7-9] Most recent models recognize that flow at high stress is non-Newtonian (viscoelastic) and use the Eyring model for shear-stress dependent viscosity.[10-14] Radial compressive and tensile hoop growth stresses are predicted for oxidation of silicon fibers.[12,15-16] Axial stresses are generally ignored.[10-11,15,17] For structural fibers this is an important omission, because axial stress has the most significant effect on fiber strength. Applied tensile stress increases oxidation rates of silicon,[18-20] and recently this has also been demonstrated for SiC fibers.[21]

A method to calculate the radial, axial, and hoop growth stress components anywhere in a SiO_2 scale formed by oxidation of SiC fibers is presented. The method involves discretization of the scale into layers and separate calculation of stresses in each layer. Calculations are done at temperatures from 700° to 1300°C for amorphous scales. Growth stresses for SiC fibers with different radii are examined. Assumptions and limitations of the method are discussed. Complementary results, along with a more thorough description of the background information and method are given elsewhere.[22]

METHOD

General

A schematic of the volume expansion and attendant stresses during SiC fiber oxidation with discretization of SiO_2 scale into annular layers is in figure 1. There are two sources of stress. The first is the initial elastic constraint of the 2.2× volume expansion accompanying oxidation of SiC to SiO_2. This expansion is shown in stress-free (dilational) and constrained states (Fig. 1). The second is the circumferential expansion of old scale as it is radially displaced outward by formation of new scale (Fig. 1). This creates tensile hoop stress (σ_θ) in the outer scale,[4,23] and tensile axial stress (σ_z) by the Poisson effect.

The large volume expansion raises concerns for growth stress modeling. Elastic constraint of the 2.2× volume expansion causes ~25 GPa compressive stress in SiO_2 for SiC oxidation, which is much larger than stresses for which linear elasticity is valid.[7] However, high shear stresses relax very rapidly to values appropriate for linear elasticity if SiO_2 viscosity is shear-stress dependent, as in the Eyring model,[10-11,24-25] and discretization to small increments can confine incremental displacements and stress differences to values appropriate for linear theory.[13,26-27]

General models of oxidation growth stress are coupled diffusion-reaction and fluid-mechanical problems.[26] The oxygen diffusion rate drives the rate that stress in the oxide is generated. Stress, in turn, affects the oxygen diffusion rates. The measured oxidation rates for SiC, whether they are flat plates, fibers, or particles, inherently include the effect of growth stress; stress-free oxidation rates cannot be measured. The effect of stress on oxidation rate will therefore not initially be considered when modeling growth stress.

The following assumptions are used in modeling the growth stress:

1. Oxidation volume expansion is dilational.
2. Stresses resulting from constraint of oxidation expansion are relaxed by flow of SiO_2 with shear stress-dependent viscosity.
3. Discretization of oxidation to small increments allows use of linear elasticity.
4. Growth stress effects on oxidation kinetics are not considered.
5. Stress relaxation in the SiC fiber is negligible.

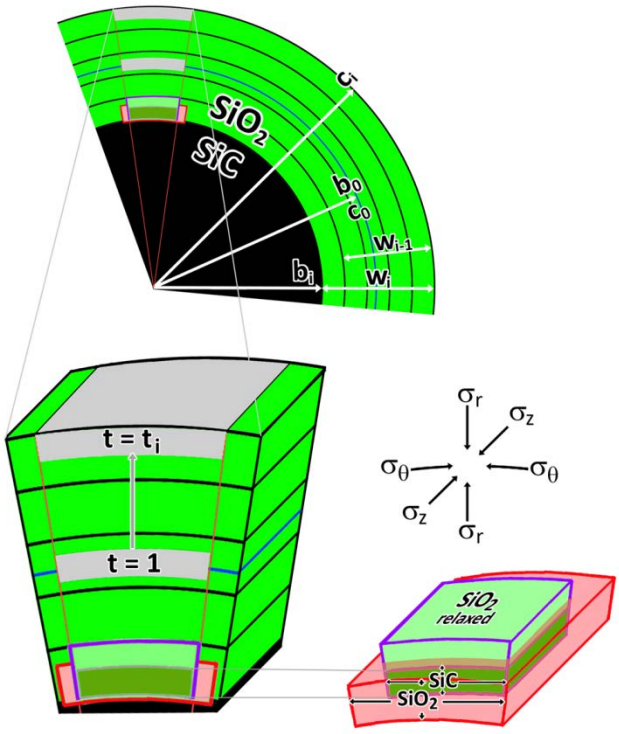

Fig. 1. *Schematic diagrams of oxidation of SiC to SiO_2. The original SiC surface is a blue line (**c_o, b_o**), midway through the scale thickness.*

Fiber Oxidation Kinetics

Fiber oxidation kinetics will not deviate significantly from flat-plate geometry kinetics until the oxidation product for 12 μm diameter fibers is several microns thick.[1,15,28] SiO_2 thickness (**w**) (Fig. 1) therefore obeys Deal-Grove kinetics for flat-plate geometry:[1,29]

$$w = \frac{1}{2}A\sqrt{1+\frac{4Bt}{A^2}} - 1 \qquad [1]$$

The parabolic and linear rate constants are **B** and **B**/**A**, respectively. **B** and **A** obey the usual Arrhenius relationships:

$$\mathbf{A} = A_0 e^{\frac{-Q_A}{RT}} \qquad [2]$$

$$\mathbf{B} = B_0 e^{\frac{-Q_B}{RT}} \qquad [3]$$

where **T** is absolute temperature, **R** is the gas constant, $\mathbf{Q_A}$ and $\mathbf{Q_B}$ are activation energies and $\mathbf{A_o}$ and $\mathbf{B_o}$ are pre-exponential factors. The SiC radius (**b**) after oxidation is (Fig. 1):

$$\mathbf{b} = \sqrt{w^2(\Omega^2 - \Omega) + b_o^2} - \Omega w \qquad [4]$$

where $\mathbf{b_o}$ is the original fiber radius and **Ω** is the ratio of SiC/SiO_2 molar volume ratio. The outer radius of the SiO_2 scale (**c**) is (Fig. 1):

$$\mathbf{c} = b+w \qquad [5]$$

Elastic Growth Stress

The elastic stresses and strains are determined by modification of a method used for sequentially deposited coatings.[30] For discretized fiber oxidation, the "deposition" sequence is reversed; the last oxide increment forms at the SiC-SiO_2 interface, and the oldest is at the surface. The system is divided into the unoxidized SiC fiber, the SiO_2 added from time **t**(i -1) to **t**(i) at the SiC-SiO_2 interface, and the outer SiO_2 increment added from **t**(0) to **t**(i-1) (Fig. 1). The axial, radial, and hoop stresses in the SiC fiber at time **t**(i) are $\boldsymbol{\sigma_z^{SiC}}$(i), $\boldsymbol{\sigma_r^{SiC}}$(i) , and $\boldsymbol{\sigma_\theta^{SiC}}$(i) respectively, and in the two SiO_2 increments are $\boldsymbol{\sigma_z^{SiO2}}$(i), $\boldsymbol{\sigma_r^{SiO2}}$(i) , $\boldsymbol{\sigma_\theta^{SiO2}}$(i) and $\boldsymbol{\sigma_z^{SiO2}}$(i-1), $\boldsymbol{\sigma_r^{SiO2}}$(i-1) , $\boldsymbol{\sigma_\theta^{SiO2}}$(i-1), respectively. The increment in SiO_2 thickness formed from **t**=i-1 to **t**=i is **w**(i)-**w**(i-1). The effect of the i^{th} SiO_2 increment on growth stresses is found using strain compatibility equations, where the dilational strain is:[30]

$$\Delta\varepsilon = \sqrt[3]{\frac{1}{\Omega}} - 1 \qquad [6]$$

and

$$\sigma_z^{SiC}(i) = \frac{-E_{SiC} f}{\pi\left(E_{SiC} b^2(i) + E_{SiO_2}\left(\left(b(i) + w(i) - w(i-1)\right)^2 - b^2(i)\right)\right)} + \sigma_z^{SiC}(i-1) \qquad [7]$$

$$\sigma_r^{SiC}(i) = \sigma_r^{SiC}(i-1) - p_{is} \qquad [8]$$

$$\sigma_\theta^{SiC}(i) = \sigma_\theta^{SiC}(i-1) - p_{is} \qquad [9]$$

$$\sigma_z^{SiO_2}(i) = \frac{-E_{SiO_2} f}{\pi\left(E_{SiC} b(i)^2 + E_{SiO_2}\left(\left(b(i) + w(i)\right)^2 - b(i)^2\right)\right)} \qquad [10]$$

$$\sigma_r^{SiO_2}(i) = -p_i \qquad [11]$$

$$\sigma_\theta^{SiO_2}(i) = \frac{p_j\left(b(i) + w(i)\right)}{w(i) - w(i-1)} \qquad [12]$$

$$\sigma_z^{SiO_2}(i-1) = \frac{f}{\pi\left[\left(b(i-1) + w(i-1) - w(i)\right)^2 - b^2(i-1)\right]} \qquad [13]$$

$$\sigma_r^{SiO_2}(i-1) = 0 \qquad [14]$$

$$\sigma_\theta^{SiO_2}(i-1) = \frac{2p_{is} b(i-1)^2 - p_i\left(\left(b(i-1) + w(i-1)\right)^2 + b(i-1)^2\right)}{\left(b(i-1) + w(i-1)\right)^2 - b(i-1)^2} \qquad [15]$$

where **f** is the axial force, $\mathbf{p_{is}}$ is the pressure across the SiO_2-SiC interface, $\mathbf{p_i}$ is the pressure across the interface between the i^{th} and the $i\text{-}1^{th}$ SiO_2 increments, $\mathbf{E_{SiC}}$ and $\mathbf{E_{SiO2}}$ are Young's modulus of the SiC fiber and the SiO_2 scale, respectively, and $\boldsymbol{\nu_{sic}}$ and $\boldsymbol{\nu_{sio2}}$ are Poison's ratio for the SiC fiber and the SiO_2 scale. Stresses in older increments (j = i-2 to j = 0) are updated with the stress values in [13 - 15]:

Relaxation of Elastic Stress

The relaxation of the elastic stresses for all increments (j=1 to i) in time increment $\boldsymbol{\Delta t}$=**t**(i)-**t**(i-1) are calculated next. The Eyring model for shear-stress ($\boldsymbol{\tau}$) dependence of glass viscosity ($\boldsymbol{\eta}$) is used for SiO_2:[11-12,16,31-34]

$$\eta = \eta_o \frac{\tau\, V_c/_{2kT}}{\mathrm{Sinh}\left(\tau\, V_c/_{2kT}\right)} = \eta_o \frac{\tau/_{\tau_c}}{\mathrm{Sinh}\left(\tau/_{\tau_c}\right)} \quad [16]$$

$\mathbf{V_c}$ is the activation volume for plasticity in SiO_2.[11-12,34] $\mathbf{k}$ is Boltzmann's constant, $\boldsymbol{\tau_c}$ is the critical shear stress above which plasticity is significant (typically ~100 MPa), and $\boldsymbol{\eta_o}$ is the stress-free SiO_2 viscosity:[35-36]

$$\eta_o = C_o\, e^{\frac{Q}{RT}} \quad [17]$$

where $\mathbf{C_o}$ and $\mathbf{Q}$ are the pre-exponential factor and activation energy for stress-free viscosity, respectively.[35-36] Shear stress relaxation obeys a Maxwell viscoelastic model:[11,34,37]

$$\frac{d\tau}{dt} = -G\,\tau/_{\eta(\tau)}\,, \qquad \tau[t(i-1)] = \tau_o \quad [18]$$

where $\mathbf{G}$ is the SiO_2 shear modulus, and the initial elastic shear stress at $\mathbf{t}$(i -1) is $\boldsymbol{\tau_o}$. The relaxation of $\boldsymbol{\tau_o}$ to a new value ($\boldsymbol{\tau}$) in time increment $\boldsymbol{\Delta t}$ for all the increments (j=1 to i) is determined by substitution of [16-17] in [18] and solving differential equation [18] for $\boldsymbol{\tau}$:

$$\tau = \frac{4kT}{V_c}\mathrm{Coth}^{-1}\left[\frac{e^{\frac{Gt}{\eta_o}}}{\sqrt{\mathrm{Tanh}\left[\frac{V_c\tau_o(j)}{4kT}\right]^2}}\right] = 2\tau_c\mathrm{Coth}^{-1}\left[\frac{e^{\frac{Gt}{\eta_o}}}{\sqrt{\mathrm{Tanh}\left[\frac{\tau_o(j)}{2\tau_c}\right]^2}}\right] \quad [19]$$

$\boldsymbol{\tau_o}$ is determined from the principal stresses for all the increments (j=1 to i) by the usual method:[38]

$$\tau_o(j) = \left[\tfrac{1}{2}\, s_{ij}(j)s_{ij}(j)\right]^{1/2} \quad [20]$$

$\mathbf{s_{ij}}$(j) are the components of the deviatoric stress tensor of the j[th] annular element at time $\mathbf{t}$(i):

$$s_{ij}(j) = \sigma_{ij}(j) - \tfrac{1}{3}\delta_{ij}\,\sigma_{kk}(j) \quad [21]$$

Relaxation of $\boldsymbol{\sigma_\theta}$(j)and $\boldsymbol{\sigma_z}$(j) is proportional to $\boldsymbol{\tau}$(j)$\boldsymbol{/\tau_o}$(j) and to their difference with $\boldsymbol{\sigma_r}$(j), which is a boundary condition, being zero at the SiO_2 surface and near zero elsewhere. The relaxed values of $\boldsymbol{\sigma_\theta}$(j)and $\boldsymbol{\sigma_z}$(j) ($\boldsymbol{\sigma_\theta}(j)'$ and $\boldsymbol{\sigma_z}(j)'$) are determined by solution of:

$$\begin{bmatrix}\sigma_\theta(j)' & 0\\ 0 & \sigma_z(j)'\end{bmatrix} = \frac{\tau(j)}{\tau_o(j)}\begin{bmatrix}\sigma_\theta(j)-\sigma_r(j) & 0\\ 0 & \sigma_z(j)-\sigma_r(j)\end{bmatrix} + \begin{bmatrix}\sigma_r(j) & 0\\ 0 & \sigma_r(j)\end{bmatrix} \quad [22]$$

Radial Displacement and Hoop Stress Generation

Relaxation expands the SiO_2 scale radially. The individual radial displacement of the j[th] increment ($\mathbf{u_r}$) is:

$$u_r(j) = \frac{\Omega_{SiO_2}}{\Omega_{SiC}\left(1+\varepsilon_z^{SiO2}(j)+\varepsilon_\theta^{SiO2}(j)+\varepsilon_z^{SiO2}(j)\varepsilon_\theta^{SiO2}(j)\right)} - 1 \quad [23]$$

where

$$\varepsilon_z^{SiO2}(j) = \frac{1}{E_{SiO_2}}\left[\sigma_z^{SiO2}(j) - \upsilon_{SiO_2}\left(\sigma_\theta^{SiO2}(j)+\sigma_r^{SiO2}(j)\right)\right] \quad [24]$$

$$\varepsilon_\theta^{SiO2}(j) = \frac{1}{E_{SiO_2}}\left[\sigma_\theta^{SiO2}(j) - \upsilon_{SiO_2}\left(\sigma_z^{SiO2}(j) + \sigma_r^{SiO2}(j)\right)\right] \quad [25]$$

The total radial displacement of the j^{th} increment is the sum of the displacements of younger increments. This adds hoop strain ($\boldsymbol{\varepsilon_\theta^{SiO2}}$) to outer layers as they are forced to a larger circumference (Fig. 1). The new hoop strain in each increment is:

$$\varepsilon_\theta^{SiO2}(j)' = \varepsilon_\theta^{SiO2}(j) + \sum_j^i u_r(j)\frac{b(j-1) - b(j)}{b(j)} \quad [26]$$

Recalculation of Elastic Stress in the Scale and SiC Fiber after Radial Displacement

The stresses in each SiO_2 increment are recalculated for $\boldsymbol{\varepsilon_\theta^{SiO2}}(j)'$ by solving the three strain compatibility equations for the three principal stresses. Revised axial stress $\boldsymbol{\sigma_z^{SiC}}$ is computed from the force exerted by the SiO_2 scale, which is the sum of the axial stress in each SiO_2 increment × area of that increment:

$$\sigma_z^{SiC}(i) = -\sum_{j=1}^{i-1}\frac{\sigma_z^{SiO2}(j)[2c(i)(w(j) - w(j-1) + w(j)^2 - w(j+1)^2]}{b(i)^2} \quad [27]$$

The revised radial and hoop stress in the SiC fiber are calculated by determining the net pressure ($\mathbf{p_n}$) from the sum of the pressures in each annular increment:

$$\sigma_r^{SiC}(i) = \sigma_\theta^{SiC}(i) = -p_n = -\sum_{j=1}^{i-1}\sigma_\theta^{SiO2}(j)\frac{w(j) - w(j-1)}{b(i)} \quad [28]$$

These revised stresses are added to the next increment i as the program loops back to equations [1 -28]. For SiC oxidation when **w(i)** << **b(i)**, the stress in SiC is much smaller than that in SiO_2.

RESULTS AND DISCUSSION

General

Growth stress calculations were done using [1-28] in a Mathematica™ program using scale discretization to 500 layers (i=500). Calculations were done for oxidation of Hi-Nicalon™-S SiC fiber for amorphous scales of 10, 100, 300, 1000, and 3000 nm thickness (**w**) at 700, 800, 900, 1000, 1100, 1200, and 1300°C. The Deal-Grove oxidation kinetics for this fiber have been reported for dry air between 700 and 1300°C, with $\mathbf{A_o} = 6.5 \times 10^{-4}$ m, $\mathbf{B_o} = 1.2 \times 10^{-8}$ m^2/s, $\mathbf{Q_A}$ = 111 kJ/mol, and $\mathbf{Q_B}$ = 249 kJ/mol.[1,39] The initial fiber radius ($\mathbf{b_0}$) is 6.1 μm. The molar volumes for SiC ($\boldsymbol{\Omega_{SiC}}$) and amorphous SiO_2 ($\boldsymbol{\Omega_{SiO2}}$) are 27.34 cm^3 and 12.46 cm^3, respectively. The Young's modulus (**E**) and Poisson's ratio ($\boldsymbol{\nu}$) values used for SiC and SiO_2 were $\mathbf{E_{SiC}}$ = 400 GPa, $\boldsymbol{\nu_{SiC}}$ = 0.157, $\mathbf{E_{SiO2}}$ = 70 GPa, and $\boldsymbol{\nu_{SiO2}}$ = 0.17. The shear modulus for silica (**G**) is 34 GPa, and has only weak temperature dependence.[40] The pre-exponential factor $\mathbf{C_o}$ and activation energy **Q** for stress-free SiO_2 viscosity are 3.8×10^{-13} Pa·s and 712 kJ/mol, respectively.[35-36] The activation volume for plasticity in SiO_2, $\mathbf{V_c}$, decreases with temperature, and has been inferred to have values ranging from 1.2×10^{-28} m^3 to 3×10^{-28} m^3.[11-12,34] $\mathbf{V_c}$ corresponds to a critical shear stress $\boldsymbol{\tau_c}$ of about 100 MPa, which is roughly consistent with experiment at 500 to 1400°C.[32,41] The variation in growth stress with change in fiber radius was examined by calculations using $\mathbf{b_o}$ = 2 μm and "flat-plate" $\mathbf{b_0} \rightarrow \infty$ (1 km). Calculations for $\boldsymbol{\sigma_\theta}$, $\boldsymbol{\sigma_z}$, $\boldsymbol{\sigma_r}$, and $\boldsymbol{\tau}$ at **T** of 700° - 1300°C for w = 300 nm and $\mathbf{b_o}$ = 2 μm, 6 μm, and "flat-plates" are shown in figure 2. Calculations for other scale thicknesses and for crystallized scales are reported elsewhere.[22]

The accuracy of growth stress calculations is limited by silica viscosity accuracy. Silica scales formed during SiC oxidation incorporate carbon.[42-45] Network carbon in amorphous SiO_2 stiffens the network structure, making it more viscous and less permeable to O_2.[46-48] However, SiO_2 viscosity may also be reduced by incorporation of impurities in Hi-Nicalon™-S fiber.[39]

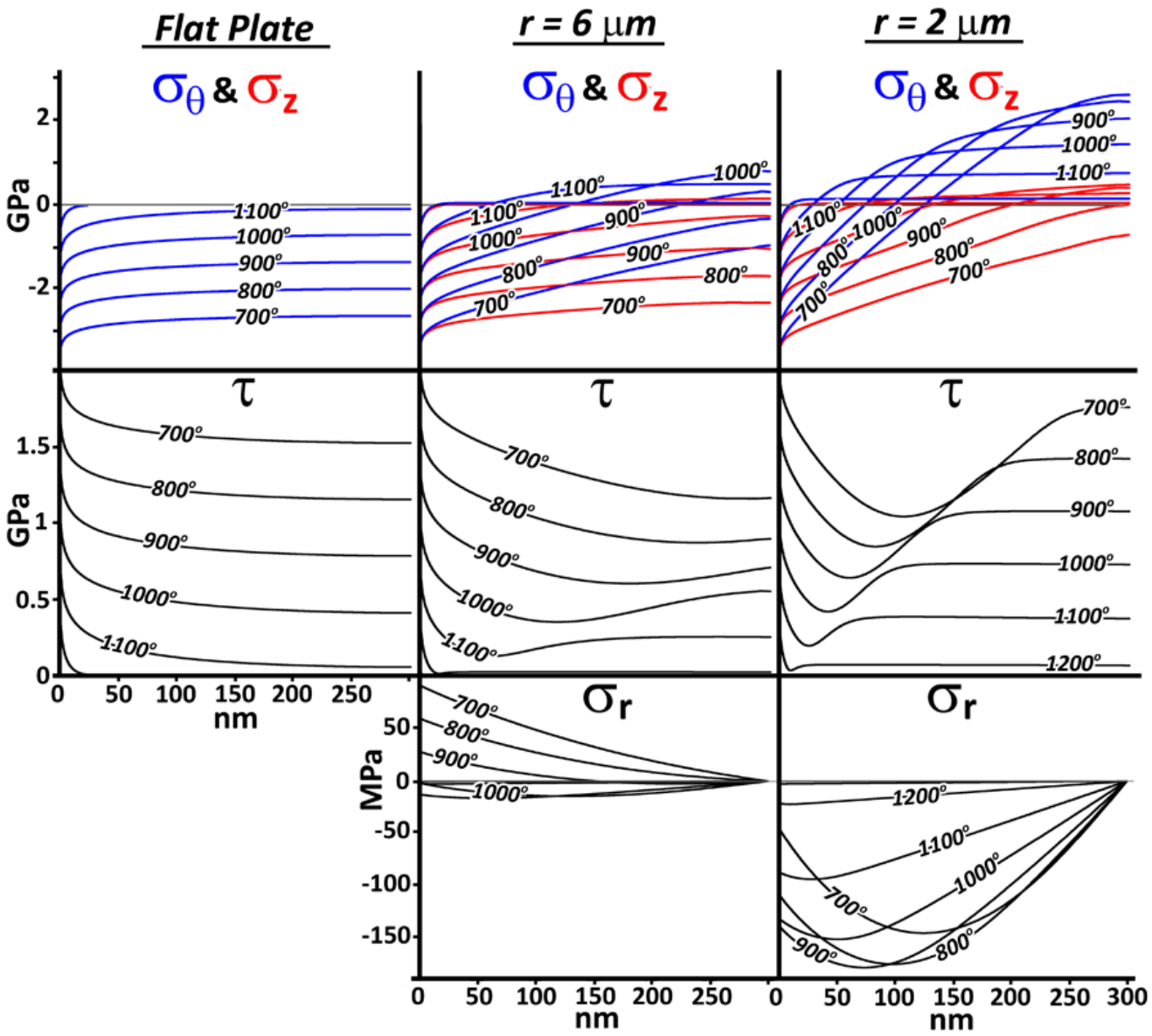

Fig. 2. *Growth stress calculations for σ_θ, σ_z, σ_r, and τ at **T** of 700°, 800°, 900°, 1000°, 1100°, 1200°, and 1300°C for a 2 μm radius fiber, 6 μm radius fiber, and a flat-plate for a 300 nm amorphous SiO_2 scale on Hi-Nicalon™-S SiC fiber.*

General features for hoop stress (σ_θ) and axial stress (σ_z) in amorphous SiO_2 scale are evident in figure 2 for 300 nm, thick scales on 2 μm and 6 μm SiC fibers and "flat-plate" SiC. The continuous changes of σ_θ and σ_z with change in $\mathbf{b_0}$ at 700°C to 1300°C throughout the scale are evident. Compressive elastic stress of ~-25 GPa for σ_θ and σ_z is rapidly relaxed by the Eyring model [16] for SiO_2 glass viscosity to ~-4 GPa at 700°C and ~-1 GPa at 1200°C just 1 nm away from the SiC-SiO_2 interface. At T >1200°C glass viscosities are so low that stress levels are insignificant more than 20 nm from the SiC-SiO_2 interface. For flat plates $\sigma_\theta = \sigma_z$, and stress is always compressive. σ_z is driven towards tensile values by the Poisson effect from the tensile σ_θ caused by outward radial expansion. Note that a 300 nm scale takes ~10^8 s to form at 700°C and ~10^5 s to form at 1000°C, so the latter is of more practical interest. Calculations for crystalline SiO_2 scale are reported elsewhere.[22] The viscosities of crystalline scale are much higher than those for amorphous scale, so growth stresses in crystalline scale are much larger than amorphous scale.

For a 2 μm radius fiber, tensile σ_θ develops at the scale surface at all temperatures, and reaches 3 GPa at 700°C. Tensile σ_z does not develop until **T** > 800°C and reaches 300 MPa at 1000°C. For a 6

μm radius fiber, tensile σ_θ does not develop until **T** > 850°C and reaches a maximum of about 600 MPa at 1000°C; tensile σ_z does not develop until **1**100°C and reaches 100 MPa at that temperature. For thicker scales, larger fractions of the scale are under tensile stress.[22]

For a 2 μm radius fiber, compressive σ_r up to -200 MPa is present in the center of the scale at 800° - 900°C. This is a consequence of tensile σ_θ at the scale surface. σ_r decreases towards the SiC-SiO_2 interface from the high compressive σ_θ near that interface. For a 6 μm radius fiber σ_r is tensile at 700° – 900°C because σ_θ is compressive at the scale surface and throughout the scale thickness, and only reaches small compressive values at T > 900°C when significant amounts of the scale are in tensile.

τ of ~12 GPa is rapidly relaxed to ~ 2 GPa at 700°C and 500 MPa at 1100°C just 10 nm away from the SiC-SiO_2 interface (Fig. 2). It continues to decrease as compressive σ_z and σ_θ decreases with distance from the SiC-SiO_2 interface until σ_θ becomes tensile, at which point τ increases towards the SiO_2 surface, reaching surface values > 1.5 GPa at 700°C for a 2 μm radius fiber and > 1 GPa for a 6 μm radius fiber, and values close to 500 MPa at 1000°C for both fiber radii..

Steady-State Tensile Stress

For the 300 nm thick scale a "steady-state" develops for σ_θ tensile stress for T > 700°C for $\mathbf{b_o}$ = 2 μm and T > 1000°C for $\mathbf{b_o}$ = 6 μm. For thicker scales the steady-state region develops at lower temperatures.[22] For $\tau < \tau_c$ of 100 MPa [16] where a stress–free viscosity (η_o) [17] is applicable, an analytical expression for the steady-state hoop stress [σ_θ(ss)] can be derived:[22]

$$\sigma_\theta\,(ss) = \frac{2B\left(\frac{1}{\Omega} - 1\right)\eta_o}{wb} \qquad [29]$$

For τ > 100 MPa the stress dependence of viscosity is significant, and η [16] must be substituted for η_o, giving:

$$\sigma_\theta\,(ss) = -2\tau_c \mathbf{Csch}\left[\frac{bw\tau_c\Omega}{B\eta_o(\Omega - 1)}\right]^{-1} \qquad [30]$$

Comparison of predictions for steady-state σ_θ(ss) tensile stress from [30] for a 6 μm radius ($\mathbf{b_o}$) fiber with numerical calculations are shown to be very close in another publication.[22]

By insetting the Arrhenius expressions for **B** and η_o into [29], the decrease in steady-state tensile stress with increasing temperature is a consequence of $\mathbf{Q} > \mathbf{Q_b}$:

$$\sigma_\theta\,(ss) = \frac{2B_oC_oe^{\frac{Q-Q_b}{RT}}\left(\frac{1}{\Omega} - 1\right)}{wb} \qquad [31]$$

If materials exist for which $\mathbf{Q} < \mathbf{Q_b}$, an increase in tensile growth stress with increase in oxidation temperature is expected.

Summary and Conclusions

A method to calculate the axial, hoop, and radial growth stresses in SiO_2 scales generated by the 2.2× volume expansion during SiC fiber oxidation was developed. The method assumes the initial oxidation volume expansion is equal in all directions (dilatational) and that the stresses resulting from constraint of that expansion are relaxed radially with an Eyring stress-dependent SiO_2 viscosity, although other appropriate viscosity models can be substituted. The method can be equally well applied to fibers of silicon or other materials. High compressive hoop and axial stresses of ~25 GPa are very quickly relaxed to much lower values at all temperatures. Radial expansion creates tensile hoop stress in the outer scale. Tensile hoop stress eventually drives axial stress to a tensile state by the Poisson effect. Tensile hoop and axial stress can reach values > 2 and 0.5 GPa, respectively for oxidation for long times at 700° - 900°C on Hi-Nicalon^{TM}-S fibers. At temperatures greater than 1200°C growth stresses are quickly relaxed to negligible levels by viscous flow of SiO_2. The accuracy of the growth stress calculation method is likely to be limited by knowledge of accurate values for amorphous silica viscosity. Tensile hoop stresses reach steady-state values that can be described by

analytical expressions. The decrease in tensile hoop growth stress with increase in oxidation temperature is a consequence of activation energy for viscous flow > activation energy for oxidation.

References

1 Hay, R. S. *et al.* Relationships between Fiber Strength, Passive oxidation and Scale Crystallization Kinetics of Hi-Nicalon^{TM}-S SiC Fibers. *Ceram. Eng. Sci. Proc.* **32**, 39-54 (2011).

2 Chollon, G. *et al.* A Model SiC-Based Fibre with a Low Oxygen Content Prepared from a Polycarbosilane Precursor. *J. Mater. Sci.* **32**, 893-911 (1997).

3 Chollon, G. *et al.* Thermal Stability of a PCS-Derived SiC Fibre with a Low Oxygen Content (Hi-Nicalon). *J. Mater. Sci.* **32**, 327-347 (1997).

4 Hsueh, C. H. & Evans, A. G. Oxidation Induced Stresses and Some Effects on the Behavior of Oxide Films. *J. Appl. Phys.* **54**, 6672-6686 (1983).

5 Morscher, G. N. & Pujar, V. V. Design Guidelines for In-Plane Mechanical Properties of SiC Fiber-Reinforced Melt-Infiltrated SiC Composites. *Int. J. Appl. Ceram. Technol.* **6**, 151-163 (2009).

6 Morscher, G. N. Tensile creep and rupture of 2D-woven SiC/SiC composites for high temperature applications. *J. Eur. Ceram. Soc.* **30**, 2209-2221 (2010).

7 Garikipati, K. & Rao, V. S. Recent Advances in Models for Thermal Oxidation of Silicon. *J. Computational Physics* **174**, 138-170 (2001).

8 Rao, V. S. & Hughes, T. J. R. On Modelling Thermal Oxidation of Silicon I: Theory. *Int. J. Numerical Methods in Engineering* **47**, 341-358, doi:10.1002/(sici)1097-0207(20000110/30)47:1/3<341::aid-nme774>3.0.co;2-z (2000).

9 EerNisse, E. P. Stress in Thermal SiO_2 during Growth. *Appl. Phys. Lett.* **35**, 8-10 (1979).

10 Rafferty, C. S. & Dutton, R. W. Plastic Analysis of Cylinder Oxidation. *Appl. Phys. Lett.* **54**, 1815-1817 (1989).

11 Sutardja, P. & Oldham, W. G. Modeling of stress effects in silicon oxidation. *Electron Devices, IEEE Transactions on* **36**, 2415-2421 (1989).

12 Delph, T. J. Intrinsic strain in SiO_2 thin films. *J. Appl. Phys.* **83**, 786-792 (1998).

13 Pomp, A., Zelenka, S., Strecker, N. & Fichtner, W. Viscoelastic Material Behavior: Models and Discretization Used in Process Simulator DIOS. *IEEE Trans. Elec. Dev.* **47**, 1999-2007 (2000).

14 Uematsu, M. *et al.* Two-dimensional simulation of pattern-dependent oxidation of silicon nanostructures on silicon-on-insulator substrates. *Solid-State Electronics* **48**, 1073-1078 (2004).

15 Kao, D.-B., McVittie, J. P., Nix, W. D. & Saraswat, K. C. Two-Dimensional Thermal Oxidation of Silicon - II. Modeling Stress Effects in Wet Oxides. *IEEE Trans. Electron. Dev.* **35**, 25-37 (1988).

16 Rafferty, C. S., Borucki, L. & Dutton, R. W. Plastic Flow During the Thermal Oxidation of Silicon. *Appl. Phys. Lett.* **54**, 1516-1518 (1989).

17 Oh, E., Walton, J., Lagoudas, D. & Slattery, J. Evolution of stresses in a simple class of oxidation problems. *Acta Mechanica* **181**, 231-255 (2006).

18 Mihalyi, A., Jaccodine, R. J. & Delph, T. J. Stress effects in the oxidation of planar silicon substrates. *Appl. Phys. Lett.* **74**, 1981-1983 (1999).

19 Yen, J.-Y. & Hwu, J.-G. Enhancement of silicon oxidation rate due to tensile mechanical stress. *Appl. Phys. Lett.* **76**, 1834-1835 (2000).

20 Yen, J.-Y. & Hwu, J.-G. Stress effect on the kinetics of silicon thermal oxidation. *J. Appl. Phys.* **89**, 3027-3032 (2001).

21 Gauthier, W., Pailler, F., Lamon, J. & Pailler, R. Oxidation of Silicon Carbide Fibers During Static Fatigue in Air at Intermediate Temperatures. *J. Am. Ceram. Soc.* **92**, 2067-2073 (2009).

22 Hay, R. S. Growth Stress in SiO_2 during Oxidation of SiC Fibers. *J. Appl. Phys.* (submitted).

23 Brown, D. K., Hu, S. M. & Morrissey, J. M. Flaws in Sidewall Oxides Grown on Polysilicon Gate. *J. Electrochem. Soc.* **129**, 1084-1089 (1982).

24 Navi, M. & Dunham, S. T. A Viscous Compressible Model for Stress Generation/Relaxation in SiO_2. *J. Electrochem. Soc.* **144**, 367-371 (1997).

25 Hu, S. M. Stress-related Problems in Silicon Technology. *J. Appl. Phys.* **70**, R53-R80 (1991).

26 Causin, P., Restelli, M. & Sacco, R. A Simulation System Based on Mixed-hybrid Finite Elements for Thermal Oxidation in Semiconductor Technology. *Computer Methods in Applied Mechanics and Engineering* **193**, 3687-3710 (2004).

27 Senez, V., Collard, D., Ferreira, P. & Baccus, B. Two-dimensional Simulation of Local Oxidation of Silicon: Calibrated Viscoelastic Flow Analysis. *IEEE Trans. Elec. Dev.* **43**, 720-731 (1996).

28 Wilson, L. O. & Marcus, R. B. Oxidation of Curved Silicon Surfaces. *J. Electrochem. Soc.* **134**, 481-490 (1987).

29 Deal, B. E. & Grove, A. S. General Relationships for the Thermal Oxidation of Silicon. *J. Appl. Phys.* **36**, 3770-3778 (1965).

30 Tsui, Y. C. & Clyne, T. W. An Analytical Model for Predicting Residual Stresses in Progressively Deposited Coatings Part 2: Cylindrical Geometry. *Thin Solid Films* **306**, 34-51 (1997).

31 Eyring, H. Viscosity, Plasticity, and Diffusion as Examples of Absolute Reaction Rates. *J. Chem. Phys.* **4**, 283-291 (1936).

32 Donnadieu, P. P., Jaoul, O. & Kleman, M. Plasticit de la silice amorphe de part et d'autre de la transition vitreuse *Philos. Mag. A* **52**, 5-17 (1985).

33 Uchida, T. & Nishi, K. Formulation of a Viscoelastic Stress Problem Using Analytical Integration and Its Application to Visocelastic Oxidation Simulation. *Jap. J. Appl. Phys.* **40**, 6711-6719 (2001).

34 Senez, V., Collard, D., Baccus, B., Brault, M. & Lebailley, J. Analysis and Application of a Viscoelastic Model for Silicon Oxidation. *J. Appl. Phys.* **76**, 3285-3295 (1994).

35 Doremus, R. H. Viscosity of Silica. *J. Appl. Phys.* **92**, 7619-7629 (2002).

36 Hetherington, G., Jack, K. H. & Kennedy, J. C. Viscosity of Vitreous Silica. *Phys. Chem. Glasses* **5**, 130-136 (1964).

37 Malvern, L. E. *Introduction to the Mechanics of a Continuous Medium*. 1st edn, 713 (Prentice-Hall, 1969).

38 Frost, H. J. & Ashby, M. F. *Deformation Mechanism Maps.* (Pergamon Press, 1982).

39 Hay, R. S. *et al.* Hi-Nicalon^{TM}-S SiC Fiber Oxidation and Scale Crystallization Kinetics. *J. Am. Ceram. Soc.* **94**, 3983-3991 (2011).

40 Polian, A. & et al. Elastic properties of a-SiO_2 up to 2300 K from Brillouin scattering measurements. *Europhys. Lett.* **57**, 375 (2002).

41 Li, J. H. & Uhlmann, D. R. The flow of glass at high stress levels: I. Non-Newtonian behavior of homogeneous 0.08 $Rb_2O{\cdot}0.92$ SiO_2 glasses. *J. Non. Cryst. Sol.* **3**, 127-147 (1970).

42 Narushima, T., Kato, M., Murase, S., Ouchi, C. & Iguchi, Y. Oxidation of Silicon and Silicon Carbide in Ozone-Containing Atmospheres at 973K. *J. Am. Ceram. Soc.* **85**, 2049-2055 (2002).

43 Chaudhry, M. I. A Study of Native Oxides of b-SiC Using Auger Electron Spectroscopy. *J. Mater. Res.* **4**, 404-407 (1989).

44 Ramberg, C. E., Cruciani, G., Spear, K. E., Tressler, R. E. & Ramberg, C. F. Passive-Oxidation Kinetics of High-Purity Silicon Carbide from 800 to 1100 C. *J. Am. Ceram. Soc.* **79**, 2897-2911 (1996).

45 Ogbuji, U. J. T. & Opila, E. J. A Comparison of the Oxidation Kinetics of SiC and Si_3N_4. *J. Electrochem. Soc.* **142**, 925-930 (1995).

46 Renlund, G. M., Prochazka, S. & Doremus, R. H. Silicon Oxycarbide Glasses: Part II. Structure and Properties. *J. Mater. Res.* **6**, 2723-2734 (1991).

47 Rouxel, T., Massouras, G. & Soraru, G.-D. High Temperature Behavior of a Gel-Derived SiOC Glass: Elasticity and Viscosity. *J. Sol-Gel Sci. Tech.* **14**, 87-94 (1999).

48 Rouxel, T., Soraru, G.-D. & Vicens, J. Creep Viscosity and Stress Relaxation of Gel-Derived Silicon Oxycarbide Glasses. *J. Am. Ceram. Soc.* **84**, 1052-1058 (2001).